5 Magnetic domains

As stated in section 1.2.2 ultrathin Ni/Cu(100) films are magnetized in-plane between 5 ML and 9 ML at room temperature. In section 5.1 the formation of in-plane magnetized domains is studied in detail. The internal structure of a Néel wall is analyzed, and the wall profile is compared with theoretical calculations. In section 5.2 the domain evolution of ultrathin Fe/Cu(100) as a function of the thickness is discussed. This evolution is compared with the formation of magnetic domains of Fe grown on a perpendicularly magnetized Ni/Cu(100) film in section 5.3.

5.1 5 to 8 ML Ni on Cu(100)

5.1.1 Comparison of domains at 100 K and 300 K

At 300 K the onset of ferromagnetic order was found to occur around 5 ML Ni/Cu(100) in agreement with the well-established phasediagram [33,85] shown in Fig. 1.7. Below 5 ML the Ni film is in the paramagnetic state, since the Curie-temperature T_C, below which the magnetic moments order ferromagnetically, decreases with decreasing film thickness. In this thickness regime no in-plane or out-of-plane magnetic contrast (MC) was observed by SPLEEM. Around 5 ML Ni the Curie-temperature has reached 300 K, and the ferromagnetic order within the film plane is revealed by the appearance of magnetic contrast in the SPLEEM image. At the same thickness no MC was detected for the perpendicular component of the magnetization, indicat-

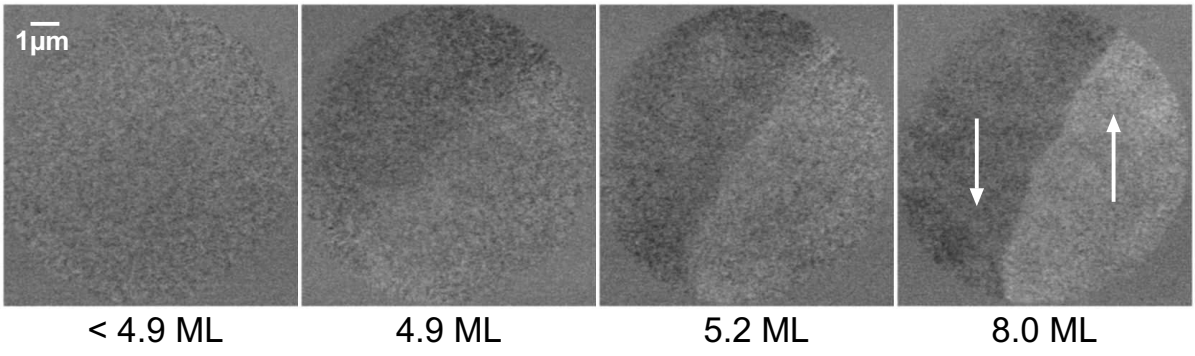

Figure 5.1: Onset of ferromagnetic order within the film plane around 5 ML Ni on Cu(100) and increasing magnetic contrast up to 8 ML Ni at 300 K. The arrows indicate the direction of the magnetization. No magnetization component perpendicular to the film plane was detected. The field of view is 10 μm.

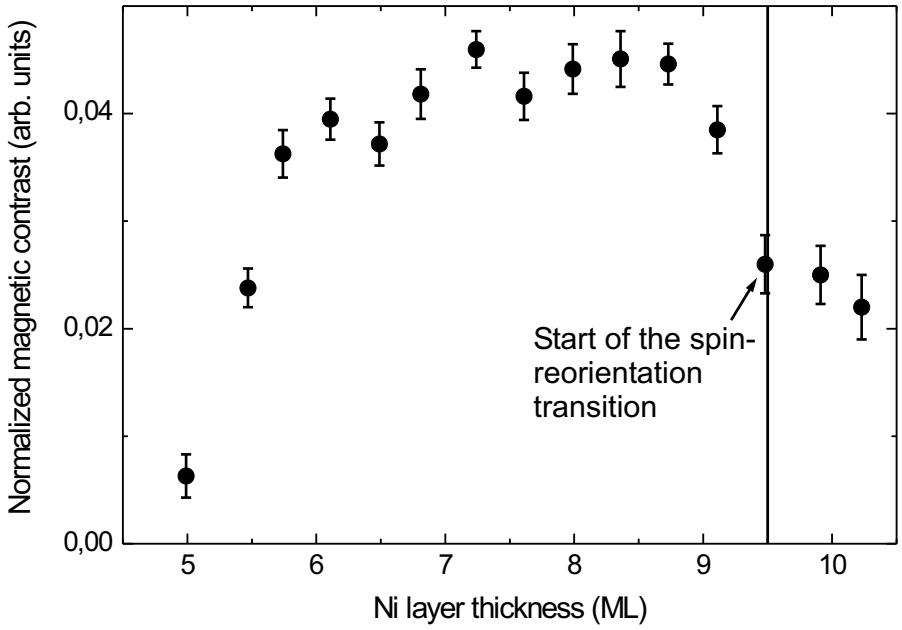

Figure 5.2: Normalized magnetic contrast of the in-plane magnetized domains of Ni/Cu(100) as a function of the Ni layer thickness. The MC increases monotonically up to about 8.5 ML Ni/Cu(100). With the start of the spin-reorientation transition at 9.5 ML the MC decreases.

ing that the magnetization was oriented parallel to the surface of the film. This is depicted in Fig. 5.1. Interestingly, no formation of smaller magnetic domains at the onset of the ferromagnetic order like in ultrathin Fe/Cu(100) (section 5.2) was observed, when the film thickness was increased in 0.1-ML steps across the critical thickness (about 4.9 ML) for ferromagnetism at 300 K. The position and the structure of the domain wall remained unchanged during subsequent deposition of additional Ni up to a thickness of 8 ML. For a film grown at 100 K the onset of ferromagnetic order was observed at lower thickness in agreement with the magnetic phasediagram of Ni/Cu(100).

As the Ni/Cu(100) film grows, the magnetic contrast increases monotonically up to about 8.5 ML Ni/Cu(100) due to the increasing number of magnetic moments contributing to the magnetization of the sample. This is demonstrated in Fig. 5.2. However, only up to 7 ML Ni the expected linear increase of the MC according to $MC \propto \mathbf{P} \cdot \mathbf{M}$ is observed. Between 7.5 and 8.5 ML the MC can also be regarded as constant within error bars, and it drops around 9 ML as the spin-reorientation transition starts (see section 6.1). The opposite orientation of the magnetization in the two adjacent domains in Fig. 5.1, which are separated by a $180°$-Néel wall, is indicated by the white arrows in the image and will be discussed in the next section in detail.

Scanning over a 2×2 mm^2 area of the surface of many in-plane magnetized Ni/Cu(100)

films of thicknesses between 4 and 8 ML the average domain size was found to be several $10\ \mu$m, substantially larger than the 10-μm maximum field of view. No statistically significant difference between the domain sizes and shapes of room temperature (RT)-grown and RT-measured films, RT-grown films measured at 100 K (low temperature, LT) and LT-grown and LT-measured films was found. In Fig. 5.3 an example of a 4.8 ML RT-grown Ni/Cu(100) measured *in situ* at 100 K is shown. For maximum contrast the polarization $\mathbf{P}$ of the electron beam was rotated within the film plane. For $\mathbf{P}$ perpendicular to the film plane no MC was observed, confirming the in-plane orientation of $\mathbf{M}$. This microscopic observation of in-plane magnetization is in good agreement with earlier findings [85]. To confirm that the SPLEEM images of the domain boundaries are representative of typical configurations, domain walls were traced over extended distances. In Fig. 5.3 the imaged area (circles) was moved in several steps to trace the domain wall. The correct alignment of the magnetic images was unambiguously verified by comparing surface step patterns in the corresponding LEEM images, which are demonstrated next to the SPLEEM images. Close inspection of the "spin-up" and "spin-down" LEEM topographic images and comparison with the corresponding magnetic images reveals no correlation between the topography of the Ni film and its magnetic domain structure. No evidence for domain wall pinning at atomic step bands was found. Comparing the images of Figs. 5.1 and 5.3 one observes a difference in the smoothness of the domain walls but no change in the domain size. The increased wall roughness of the film measured at 100 K (Fig. 5.3) is attributed to two effects: (a) when cooling from 300 K to 100 K at a base pressure of 1.5×10^{-8} Pa trace amounts of residual gases like CO and CO_2 may adsorb, which reduce the total magnetic anisotropy in the 5 ML regime considerably and (b) the formation of a zigzag domain wall which is not completely resolved. Such domain walls are known to originate from "head-on" 180°-domain walls [182], in which the magnetization vectors of the adjacent domains point to each other in an antiparallel alignment. These domain walls develop a zigzag shape in order to reduce the magnetic charge density. A straight wall would have the strongest charge concentration [17]. The SPLEEM apparatus, however, does not provide the high resolution (<5 nm) to resolve fine details of the domain wall structure as for example spin-polarized scanning tunnelling microscopy (SP-STM) techniques do (see e. g. [131]).

The systematic investigation of the domain wall width as a function of the Ni thickness at 300 K reveals a decrease in width from the onset of MC with increasing layer thickness up to 8 ML as shown in Fig. 5.4. The width of a 180° wall is theoretically given by $w_{180^\circ} = 2\sqrt{A/K_2^{\text{eff}}}$ [17], (see section 1.3.2). The error bars in Fig. 5.4 arise from the noise of each domain profile extracted from the SPLEEM images. Each profile consisting of the average of 50 parallel profile lines was taken at the same part of the domain wall as indicated in the inset of Fig. 5.4. The solid line in the figure is a guide to the eye. The domain wall width is also plotted versus the reciprocal thickness in the inset of the figure. The decrease of the width of the domain wall

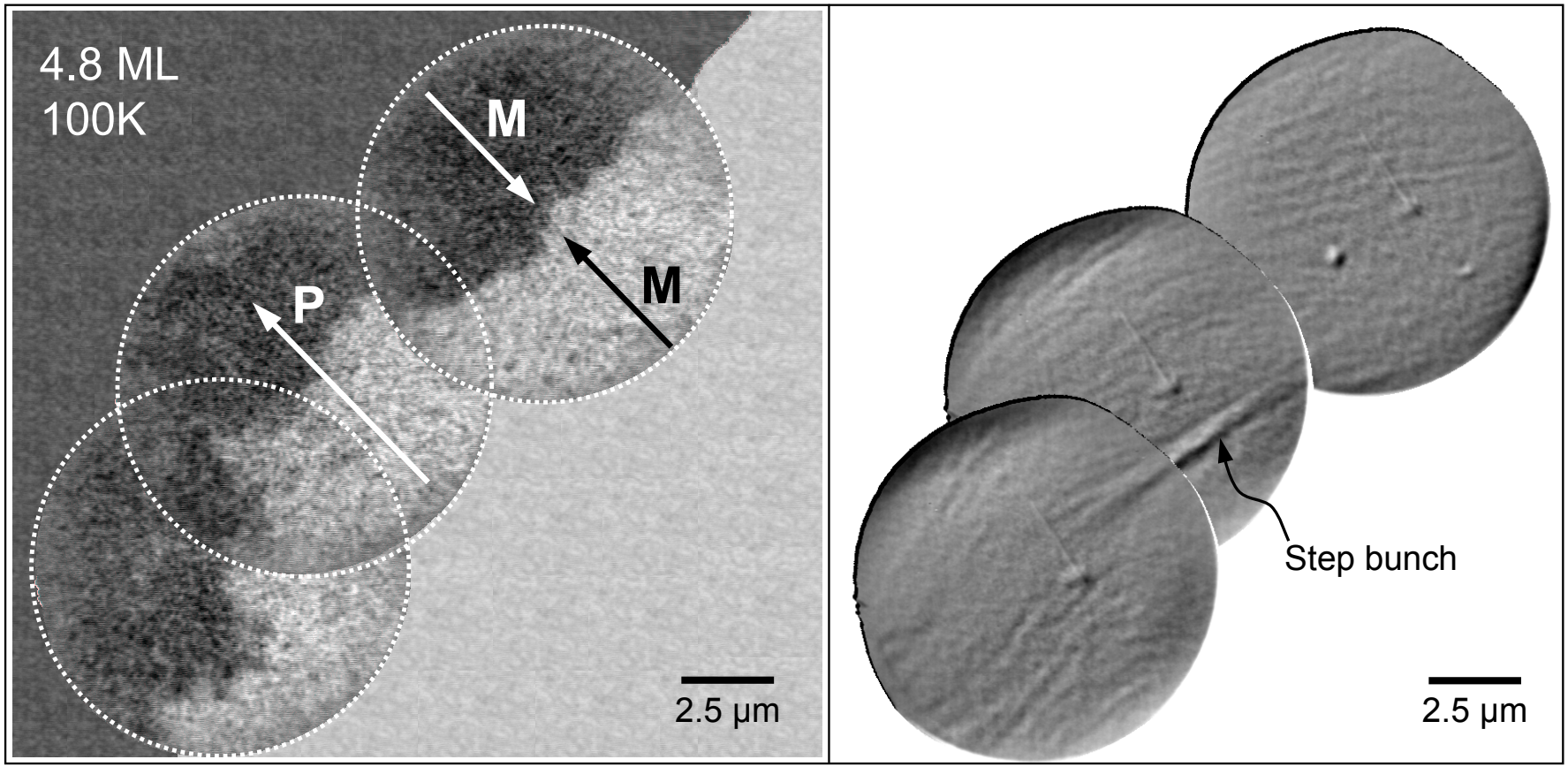

Figure 5.3: Left: Three SPLEEM images with 10-μm field of view (circles) tracing a domain wall of a 4.8 ML Ni film prepared at 300 K and measured at 100 K. The domains have several 10 μm extension. The zigzag wall structure originates from a "head-on" domain configuration (see text). Right: With the aid of the three corresponding LEEM images the correct alignment of the domain images is found by exploiting topographic features like the marked step bunch. No preferred direction or pinning of the domain wall with respect to the step edges was found.

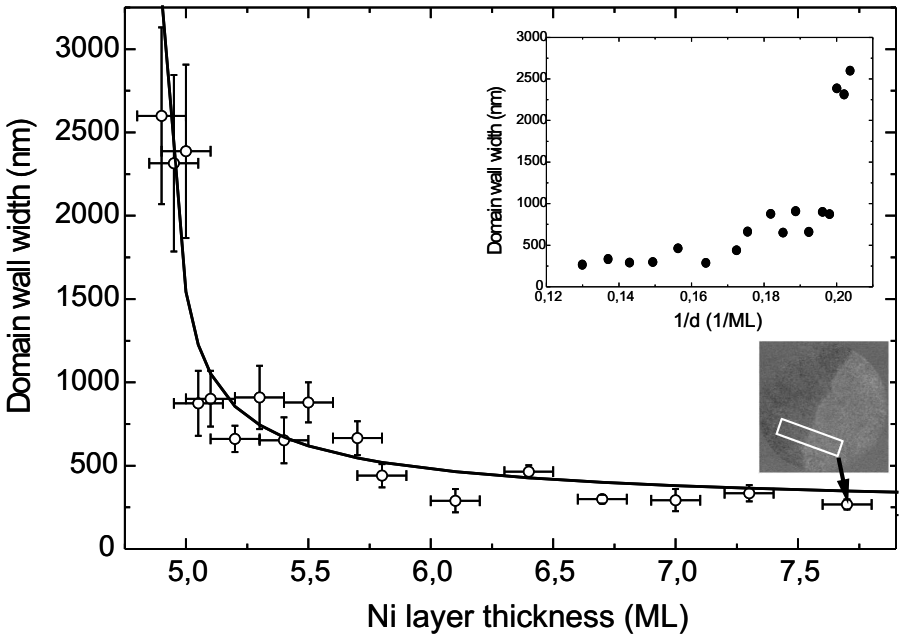

Figure 5.4: Width of the domain wall of in-plane magnetized ultrathin Ni/Cu(100) films as a function of the thickness at 300 K. The expected decrease in wall width with increasing film thickness d is due to the decrease of the surface anisotropy contribution $2K_2^S/d$. The solid line is a guide to the eye. The inset shows the width of the wall versus the reciprocal thickness.

with increasing Ni layer thickness can be understood in terms of an increase of the effective anisotropy constant $K_2^{\text{eff}} = K_2^V + 2K_2^S/d - K_d$. Since $2K_2^S/d$ is negative and large at small thicknesses, K_2^{eff} is small around 5 ML, where the domain formation sets in, leading to an extended width of the domain wall according to $w_{180^\circ} = 2\sqrt{A/K_2^{\text{eff}}}$. As the thickness of the Ni layer increases, the surface contribution $2K_2^S/d$ to K_2^{eff} decreases. Hence, the resulting increase of K_2^{eff} causes a narrowing of the domain wall. Applying $w_{180^\circ} = 2\sqrt{A/K_2^{\text{eff}}}$ as a fit function to the experimental data fails, if the previously determined anisotropy contributions $K_d = 7.5$ μeV/atom [9], $2K_2^S = -166$ μeV/atom [83] and $K_2^V = 30$ μeV/atom [37] to K_2^{eff} are used. The calculated widths of the domain wall are more than one order of magnitude too small, indicating that the assumed K_2^{eff} is too large, or that the theoretical approach is not valid for systems, like the tetragonally distorted ultrathin Ni/Cu(100) films. In order to obtain a better understanding of the Néel walls of in-plane magnetized Ni/Cu(100) films, the domain wall of a film of 8 ML thickness was analyzed in detail.

5.1.2 Analysis of a domain wall of an 8 ML Ni/Cu(100) film

For the following discussion of magnetization and electron spin-polarization directions, spherical coordinates are used. The polar angle is denoted as θ, which is measured against the surface normal ($\theta = 0^\circ$). The azimuthal angle Φ is measured in the counter-clockwise direction, and

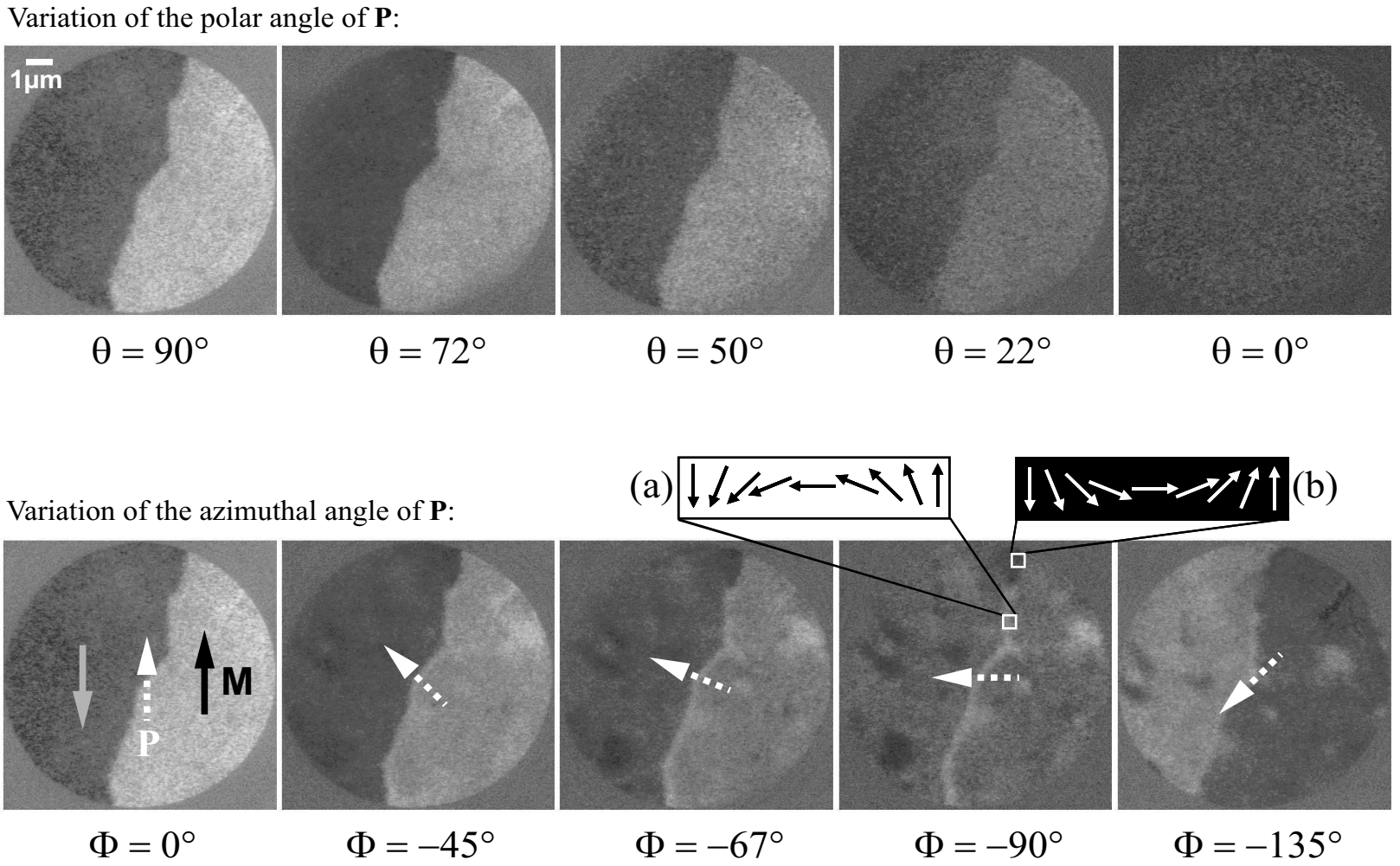

Figure 5.5: SPLEEM images of an 8 ML Ni/Cu(100) film at 300 K as a function of the polar angle θ (top) and azimuthal angle Φ (bottom) of the polarization **P** of the electron beam (white dashed arrow). Top: Sharp magnetic contrast with **P** oriented in the film plane (left), no MC with **P** normal to the surface (right), i. e. the Ni film is fully in-plane magnetized. Bottom: The MC disappears at $\Phi = -90°$, i. e. the magnetization in the domains is oriented as indicated by the arrows in the left image. Two chiralities exist in the Néel wall, as shown in the image ($\Phi = -90°$).

$\Phi = 0°$ corresponds to the "12 o'clock" orientation in the SPLEEM images.

The structure of the domain wall of the 8 ML Ni/Cu(100) film imaged in Fig. 5.1 was analyzed in greater detail as shown in Fig. 5.5. Initially, while keeping the azimuthal angle fixed at $\Phi = 0°$, the polar angle θ of the electron beam polarization was varied in steps from $\theta = 90°$ ($\mathbf{P}$ in-plane) to $\theta = 0°$ ($\mathbf{P}$ along the surface normal). Diminishing contrast in this series confirms the absence of out-of-plane magnetization components, i. e. the local magnetization vectors lie in the surface plane in both domains. Then, the polar alignment of the illumination beam polarization was fixed at $\theta = 90°$ ($\mathbf{P}$ in-plane) and the azimuthal polarization orientation was swept through an angle of $\Phi = -135°$. The magnetic contrast between the domains can be seen to decrease in this series: it finally vanishes when $\mathbf{P}$ is perpendicular to the magnetization vectors of the two domains. The absence of magnetic contrast between the two domains for the alignment $\Phi = -90°$ confirms that the two domains are anti-aligned and are thus separated by a 180° domain wall. In all but the $\Phi = 0°$ direction of $\mathbf{P}$, additional contrast can be discerned in the region of the domain wall. Most clearly at $\Phi = -90°$, a large section of the domain appears brighter and a shorter segment near the top of the image appears dark. Consequently, the domain wall has Néel structure, in which the magnetization reorientation between the two anti-aligned domains takes place within the film plane. In a Bloch wall, in which the magnetization rotates in a plane normal to the film surface, no MC would occur in the image at $\Phi = -90°$. The fact that different sections of the observed wall show opposite magnetic contrast is consistent with the expectation that Néel walls must occur in two degenerate chiralities, as indicated schematically in the figure.

To confirm this interpretation the average line profile across the 180° wall of the SPLEEM image at $\Phi = -90°$ of Fig. 5.5 (lower panel) is depicted in Fig. 5.6. The profile, consisting of the average of about 50 parallel profile lines, shows the typical shape of a Néel wall consisting of a narrow core and two long tails as discussed in reference [17]. The gray curve in the figure is a fit according to Eq. (5.2), which is based on continuum micromagnetic theory [17] and was recently applied to fit Bloch wall profiles [183]. The solid gray curve adequately describes the core of the Néel wall, yielding a width of $w_{\text{core}} \approx 400$ nm. However, this function fails in the elongated tail region of the Néel wall (dashed curve). Numerical computations yield that in the tail the direction cosine $\alpha(x)$ between the magnetization vector in the wall and the x-axis, which is assumed to be perpendicular to the easy axis of the uniaxial anisotropy of the film, decrease with the distance x from the wall center according to a logarithmic law [184,185]. The magnetic stray field originating in the tail region is shown to be responsible for the logarithmic variation. A complex analytic solution of the Néel wall shape is presented by Riedel et al. [99] which is beyond the scope of this work. For the sake of simplicity Eq. (5.3) is used to fit the tail region showing an appropriate description of the logarithmic tail of the domain wall, which is given by the black solid curve in the Fig. 5.6.

The total description of the Néel wall profile is given by Eq. (5.1), which sums up the functions for the core and the tail.

$$y_(x) = y_{core}(x) + y_{tail}(x) \tag{5.1}$$

$$y_{core}(x) = y_0 + y_1 \sin\Big(\arcsin\Big[\tanh\Big(\frac{x - x_0}{w/2}\Big)\Big] + \frac{\pi}{2}\Big), \quad -0.237\ \mu m < x < 0.237\ \mu m \tag{5.2}$$

$$y_{tail}(x) = y_{core}(x) + \ln|x|, \quad x > 0.237\ \mu m \quad \wedge \quad x < -0.237\ \mu m \tag{5.3}$$

The offset $y_0 = -141.5$ and the factor $y_1 = -6.5$ are used to fit the profile of the domain wall. Since the ordinate in Fig. 5.6 corresponds to the grey scale values determined from the SPLEEM image, there is no strict physical meaning in the values of y_0 and y_1. The fit function Eq. (5.1) rather demonstrates, that the *shape* of the Néel wall profile can be described taking a logarithmic behavior of the extended tails into account, whereas the approach for Bloch walls (Eq. (5.2)) alone is not sufficient to fit the whole Néel wall profile.

Using the equation for the width of a 180°-domain wall $w_{180°} = 2\sqrt{A/K_2^{\text{eff}}}$ with the exchange constant $A = 0.75 \times 10^{-11}$ J/m, which is the average of values given for Ni films with 157 to 250 nm thickness [186], an effective anisotropy parameter $K_2^{\text{eff}} = K_2 - K_d = 0.9 \times 10^3$ J/m^3 is derived. The parameter K_2^{eff}, which includes shape (K_d) and second-order magnetocrystalline anisotropy (K_2), is about one order of magnitude smaller than the experimental determined K_2^{eff} of an 8 ML Ni film on Cu(001) at 300 K [33,85]. Such a difference by orders of magnitude was also observed for Co monolayers on Cu(100) [187], where a Néel wall width of about 500 nm and 300 nm was measured for films of 5.5 ML and 9 ML thickness. One should note here, that a calculation of the Néel wall width of "negative anisotropy materials" favoring $\langle 111 \rangle$ directions like Ni should be corrected by taking magnetostriction effects into account, yielding a wall width $w = 6.5..7.2\sqrt{A/K_2^{\text{eff}}}$ (p. 234 of Ref. [17]) in better agreement with the experimental observations. Note, that in the SPLEEM images of the 8 ML Ni/Cu(100) film shown in Fig. 5.5 ($\Phi = -90°$, lower panel) dark and bright areas within the domains appear, indicating that the magnetization there has a different in-plane orientation than the surrounding domains. Such features have also been observed in the vicinity of the spin-reorientation transition, which starts around 9.5 ML Ni. Near the SRT the effective anisotropy is known to become very small ($<10^2$ J/m^3) [84,85], and the small K_2^{eff} derived at 8 ML Ni may be explained within this framework. To quantitatively check the theoretical predicted shape and width of domain walls in magnetic monolayers one needs accurate knowledge of the magnetic anisotropy K_2^{eff} and the exchange constant A, which turns out not to be available in many systems. For example,

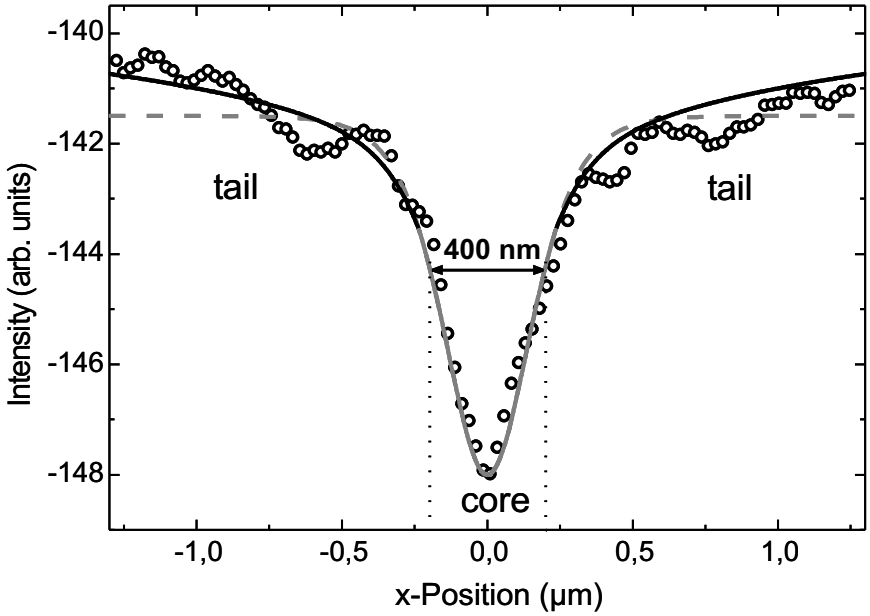

Figure 5.6: Profile of the white imaged Néel wall of the 8 ML Ni/Cu(100) film discussed in Fig. 5.5 (bottom). The gray curve is a fit according to equation 5.2. It describes adequately the 400 nm wide core of the domain wall, but it fails to fit the extended logarithmic tails of the Néel wall, which is described by equation 5.3 (black curves).

to obtain a quantitative agreement between the experimentally measured wall width of in-plane magnetized 1 ML Fe/W(110) [188] and the calculated one according to $w = 2\sqrt{A/K_2^{\text{eff}}}$, the exchange constant A had to be assumed one order of magnitude smaller than the bulk value and K_2^{eff} turned out to be more than two orders of magnitude larger than typical values of Fe films.

5.2 Evolution of magnetic stripe domains in Fe/Cu(100) films

The magnetic domains of Fe/Cu(100) ultrathin films have been observed during the film growth to investigate their evolution on a blank Cu(100) surface. The measurements have been performed at a deposition rate of 0.1 ML/min at 300 K and by using an energy of the electrons of 4.4 eV, which was optimized before, hence, to obtain the highest MC for Fe domains. Below 2.2 ML Fe no magnetic contrast was observed, which confirms that the film is in the paramagnetic state. In agreement with previous SPLEEM studies on Fe/Cu(100) films [38,169] the onset of magnetic contrast occurs around 2.2 ML Fe/Cu(100) at room temperature by the formation of anti-aligned narrow stripe domains with a perpendicularly oriented magnetization within regions of about 1 μm $\times$ 1 μm lateral size. As the Fe layer thickness is increased, both the MC

and the area in which stripe domains are formed increase within an Fe thickness interval of 0.04 ML while the stripe width remains constant. Fig. 5.7 shows the evolution of domains as a function of Fe layer thickness. At 2.22 ML the highest density of 6 stripe domains per micrometer is observed, which yields an average stripe width of 165 nm. The stripe domains run parallel to the Cu step edges and their length exceeds the field of view of the microscope which is 7 μm. Man et al. [38] observed a meandering multi domain state in the 2 ML Fe thickness range rather than ordered stripe domains. Imaging the clean Cu surface by LEEM, round step edges with no preferential direction separated by terraces of some 100 nm were observed. In contrast to their findings the stripe domains observed in this work are clearly pinned to the parallel oriented Cu steps which are separated by only $100 - 200$ nm wide terraces. Upon increasing the Fe layer thickness up to about 2.4 ML the direction of the magnetization in dark (bright) colored stripe domains, confined by adjacent bright (dark) colored stripe domains of opposite orientation of the magnetization is reversed spontaneously. This results in a formation of broader dark and bright imaged stripe domains as depicted in Fig. 5.7 (f)-(h). The maximum domain width of about 5 μm is found around 3 ML Fe/Cu(100) at room temperature [12]. Above 3 ML the domains start to form smaller stripe domains again in the vicinity of the structural transition from fct to fcc, which occurs around 3.6 ML at 300 K and is accompanied by a transition to a phase of a ferromagnetic "live layer" (not shown here).

The occurrence of magnetic contrast in Fe/Cu(100) as a function of the thickness is a consequence of the thickness dependent T_C which increases with increasing film thickness. Around 2.2 ML Fe/Cu(100) T_C reaches room temperature and ferromagnetic order sets in. Since Fe has a positive surface anisotropy, which favors an orientation of the magnetization normal to the surface and which leads to an increase of K_2 with decreasing film thickness d according to $K_2 = K_2^V + 2K_2^S/d$, the domains are perpendicularly magnetized at low thicknesses. For a 4 ML Fe/Cu(100) film the surface anisotropy $2K_2^S$ and the volume anisotropy K_2^V were determined to equal $2K_2^S = 120$ μeV/atom and $K_2^V = 78$ μeV/atom, resulting in a total $K_2 = 108$ μeV/atom at a reduced temperature $T/T_C = 0.54$ [189]. At 2.2 ML Fe K_2 is only slightly larger than the long-range dipole-dipole-interaction, which favors an in-plane orientation of the magnetization. In order to reduce the dipolar stray field energy, a domain pattern of up and down magnetized narrow stripe domains is formed at the onset of ferromagnetism. This reduction of the stray field energy, however, competes against the increase of the domain wall energy. The sinusoidal domain profile depicted in Fig. 5.8 (a) is derived from the SPLEEM image of Fig. 5.7 (e) and reflects a ratio $\delta = \frac{w}{a} = 1$ of the domain wall width w to the domain width a. In agreement with the theory stated in chapter 1.3.3 this ratio corresponds to the minimum value of the dimensionless quantity $f = f_{min} = \frac{K_2^S}{\frac{1}{2}\mu_0 M_0^2 \; a_0 \; c} \approx 1$, for which domains occur in ultrathin films. The domain configuration becomes energetically stable as f increases from f_{min}. Thus, the evolution of broader stripe domains, i. e. the degradation of domain walls, between 2.2 ML and

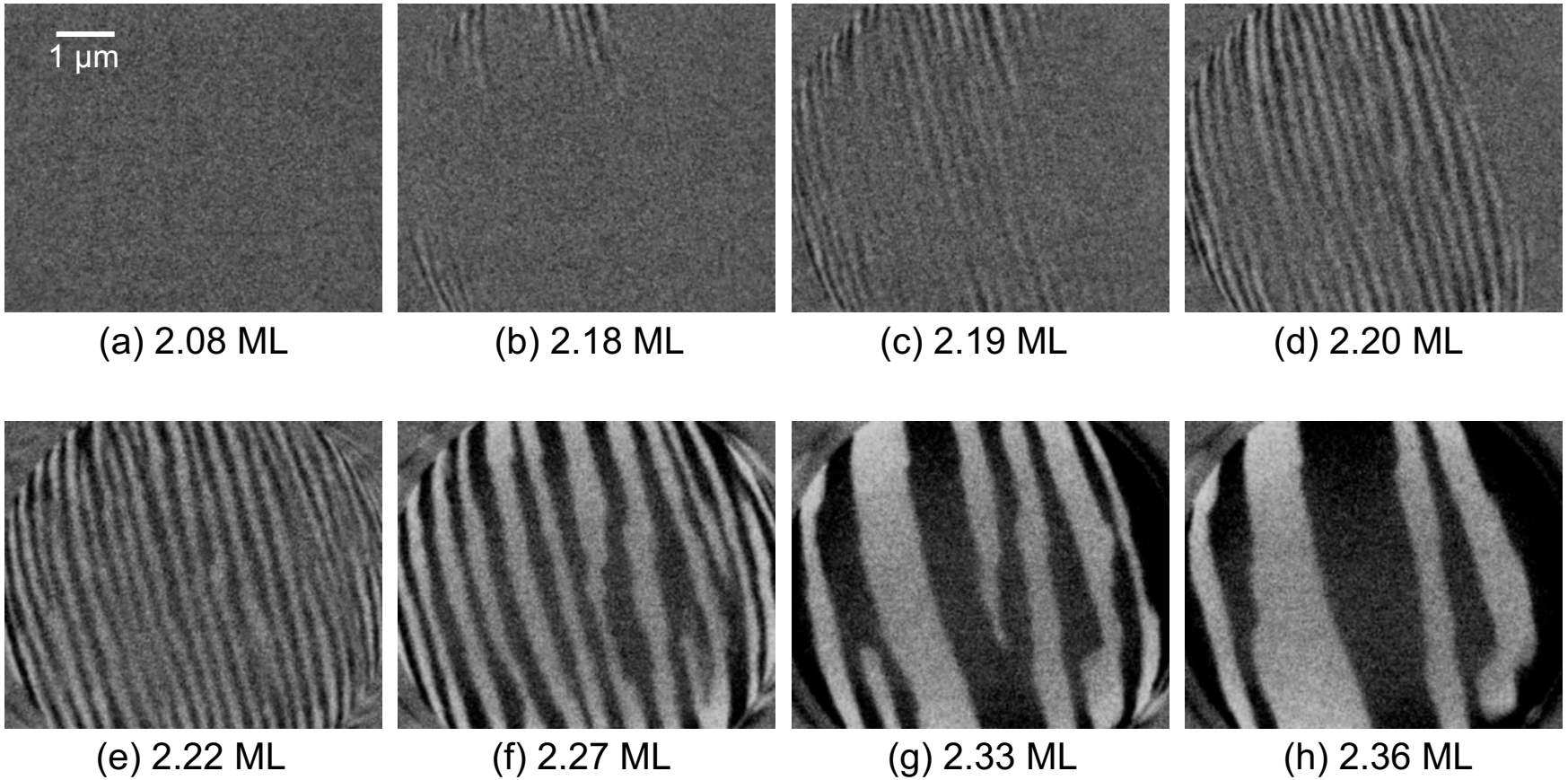

Figure 5.7: Evolution of magnetic domains of an ultrathin Fe/Cu(100) film as a function of the Fe layer thickness at 300 K. The component of the magnetization normal to the surface is imaged at an energy of the electrons of 4.4 eV. Below 2 ML the Fe film is in the paramagnetic state. At 2.2 ML Fe (b) ferromagnetic order starts by the formation of narrow, perpendicularly magnetized stripe domains. With increasing Fe layer thickness the magnetic contrast increases and the narrow stripe domains form broader domains.

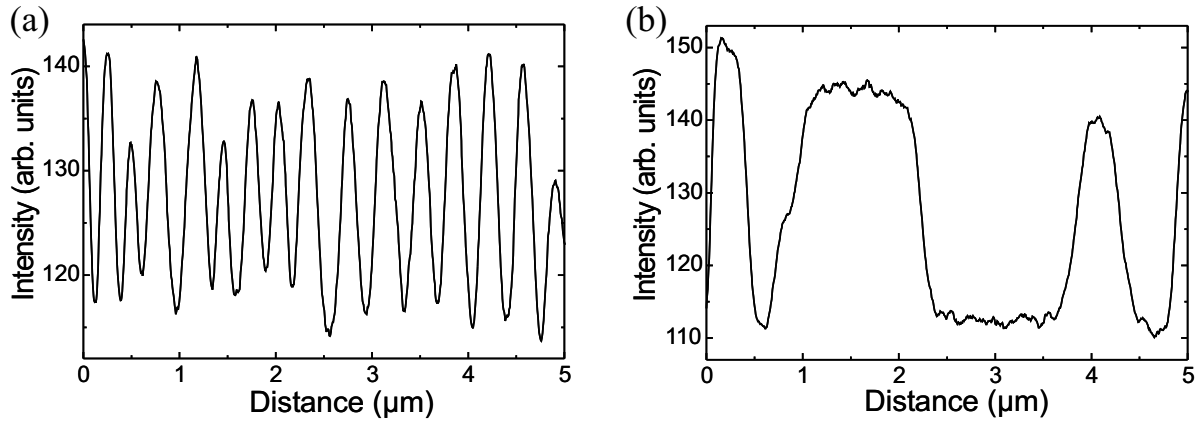

Figure 5.8: Profiles of perpendicularly magnetized stripe domains of Fe/Cu(100). (a) The profile is derived from the SPLEEM image of a 2.2 ML film shown in Fig. 5.7 (e). The average domain width is 165 nm. The sinusoidal shape reflects the equal size of domains and the separating walls and yields in agreement with theory $f = f_{min}$ (see chapter 1.3.3) for which domains occur. (b) Typical domain widths of a 2.4 ML film imaged in Fig. 5.7 (h) are 500 nm to 1500 nm.

3 ML Fe as illustrated in Fig. 5.8 (b) must be interpreted in terms of an increased K_2, indicating that in this low thickness range the proportionality $K_2 \propto \frac{1}{d}$ is obviously not valid. The domain wall energy per unit length, which is given by $\gamma = 4d\sqrt{A\,|K_2^{\text{eff}}|}$ [16], increases with increasing layer thickness d, and hence the number of domain walls is reduced. Earlier investigations of this thin film system showed again a breakup of smaller stripe domains as the Fe layer thickness is increased from 3 ML to 4 ML [12,38,169]. Here, the increase of d reduces K_2 and the multi domain state becomes energetically favorable, before K_2 becomes smaller than the shape anisotropy. This leads to a reorientation of the magnetization into the film plane around 6 ML Fe/Cu(100) grown at low temperatures [29,190].

5.3 Fe monolayers on 7 to 11 ML Ni/Cu(100)

In the previous section Fe layers were grown on a non-magnetic Cu(100) surface and the evolution of narrow stripe domains at the onset of ferromagnetism has been observed. In this section it will be demonstrated how magnetic domains evolve as Fe layers are grown on out-of-plane magnetized Ni(100) surfaces with the Cu in-plane lattice constant.

In the following chapters, again polar coordinates are used to characterize magnetization and electron spin-polarization directions, as introduced in section 5.1.2. The azimuthal angle Φ, however, is now measured against the Cu step direction as indicated in the respective figures.

5.3.1 Out-of-plane magnetized domains (0 to 2.5 ML Fe)

Fe layers up to 2.5 ML thickness were grown on out-of-plane magnetized Ni/Cu(100) films of 7 ML, 7.5 ML and 11 ML thickness. In this thickness range Ni films are still tetragonally distorted adopting the Cu in-plane lattice constant [82]. The size of the Ni domains vary between 1 μm and 6 μm, which is considerably smaller than the in-plane magnetized Ni domains at lower thicknesses which had been observed in section 5.1 to be several 10 μm. Three different Ni underlayers are discussed:

1. Ni films around 7 ML, which reveal an out-of-plane canted magnetization states with a canting angle of $20^\circ - 30^\circ$ against the surface normal.

2. Ni films around 7.5 ML, which are fully perpendicularly magnetized but still in the vicinity of the spin-reorientation transition thickness.

3. Ni films of 11 ML, which are perpendicularly magnetized and well above the SRT thickness.

The canted magnetization in 7 ML Ni/Cu(100) films yields only a weak magnetic contrast of the magnetization component normal to the surface. This is due to the small magnetic moment of Ni (0.62 μ_B) and the fact that only the component perpendicular to the film plane contributes to the signal $MC \propto \mathbf{P} \cdot \mathbf{M}$. However, the parallel alignment of the domain walls of the 7 ML Ni/Cu(100), which is the orientation of the Cu atomic step edges, can be faintly seen in Fig. 5.9. As less than 1 ML Fe is deposited onto the Ni/Cu(100) film, the domain pattern of the pure Ni film changes into a state of out-of-plane magnetized domains, which are much larger than the field of view, i. e. 7 μm . The magnetic contrast of the SPLEEM images increases as a consequence of the increased number of magnetic moments as the Fe layer grows up to 2.5 ML.

The perpendicularly magnetized domains of the 11 ML Ni/Cu(100) give rise to a strong MC, which shows that the domain walls are pinned along the substrate step edges, as compared to the topographic LEEM image in Fig. 5.10. Upon depositing Fe on top of the Ni film, again, the MC increases but the original domain pattern of the Ni film is broadened by only 20% as demonstrated in Fig. 5.9 (b). No significantly greater broadening of the original domain pattern of 11 ML Ni/Cu(100) films was observed as Fe layers were deposited up to the critical thickness, at which the spin-reorientation transition takes place. The strong domain wall pinning at the regularly aligned Cu step edges, which emerge in the LEEM image of Fig. 5.10, obviously impede the linear domain expansion in ultrathin films with large perpendicular anisotropy as found by Allenspach *et al.* [105] in Co/Au(111), or as determined by the earlier theory of Kittel [18]. There, the domain growth was found to increase with the square root of the film thickness. The domain wall width of the Ni/Cu(100) film of $w_{\text{Ni}} = 130 \pm 10$ nm increases by 15% to $w_{\text{Fe-Ni}} = 150 \pm 10$ nm by the deposition of Fe layers up to 2.3 ML. This leads to a reduction of

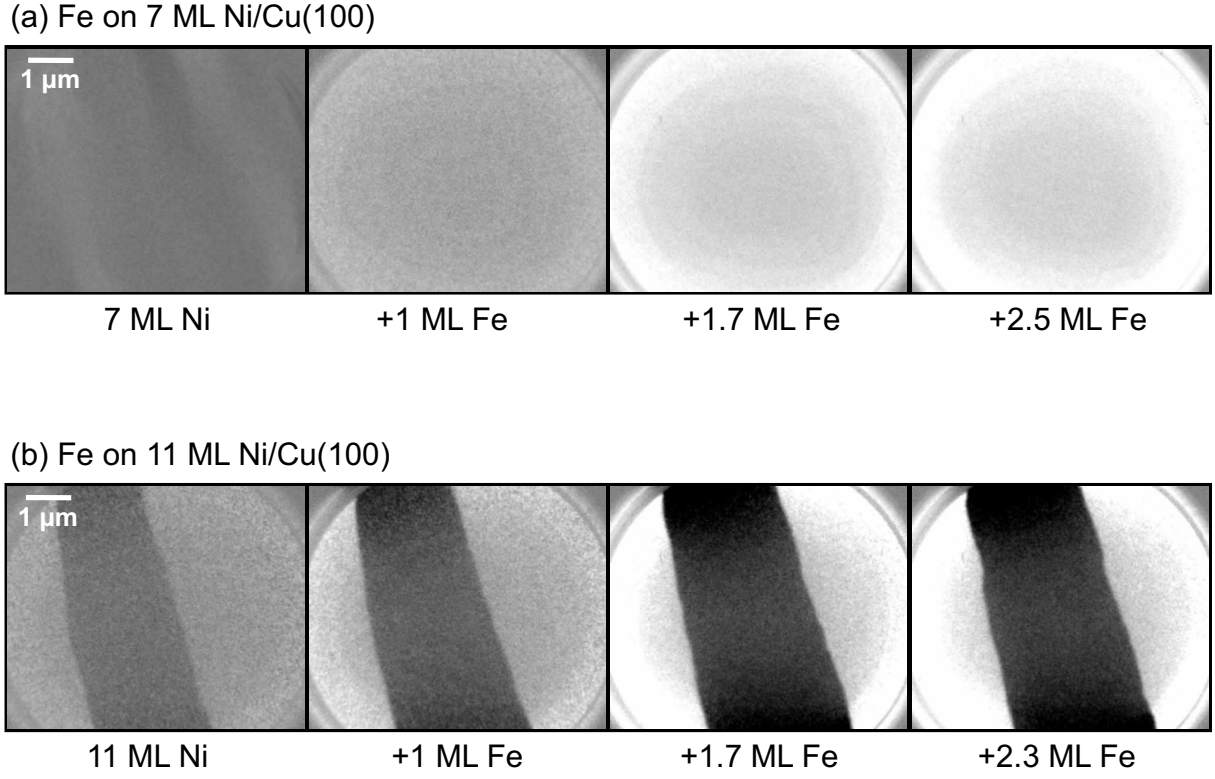

Figure 5.9: Evolution and size of magnetic domains of ultrathin Fe layers on out-of-plane magnetized Ni/Cu(100) films. The perpendicular component of the magnetization of the 7 ML Ni/Cu(100) is weak, deposition of Fe enlarges the domain size over the field of view (7 μm) and increases the magnetization dramatically (a). The magnetic contrast of the 11 ML Ni is stronger compared to 7 ML Ni and the original width of the dark imaged domain increases by only 20% (b).

the effective anisotropy K_2^{eff} including the shape anisotropy according to $w_{180^\circ} = 2\sqrt{A/K_2^{\text{eff}}}$ by 25%.

The completely perpendicularly magnetized 7.5 ML Ni/Cu(100) film reveals a domain pattern of wide stripe domains of irregular width in the range of 0.5 μm to more than 3 μm. These stripe domains are confined by domain boundaries, which are pinned at the substrate step edges as shown in Fig. 5.10. With increasing Fe layer thickness d the number of domain walls is reduced due to the enhanced wall energy given by $\gamma \propto d\sqrt{A\,|K_2^{\text{eff}}|}$. No major change of the domain wall width $w_{Ni} = 210 \pm 10$ nm of the Ni film is found during Fe deposition, indicating that K_2^{eff} does not change significantly. Up to approximately 0.5 ML Fe the residual domain walls keep pinned in there original direction, as the domain size grows beyond the 7 μm-field of view of the SPLEEM. As the Fe thickness exceeds 0.6 ML, parts of the walls detach from the pinning site. At 0.8 ML Fe the whole domain wall within the field of view has rotated counter clockwise by -30° degrees away from the initial orientation into the [011] direction, which is confirmed by the LEED image, which shows the cubic lattice structure of the bare Cu(100) crystal. Compared to the 11 ML Ni/Cu(100) the conclusion is, that the larger perpendicular

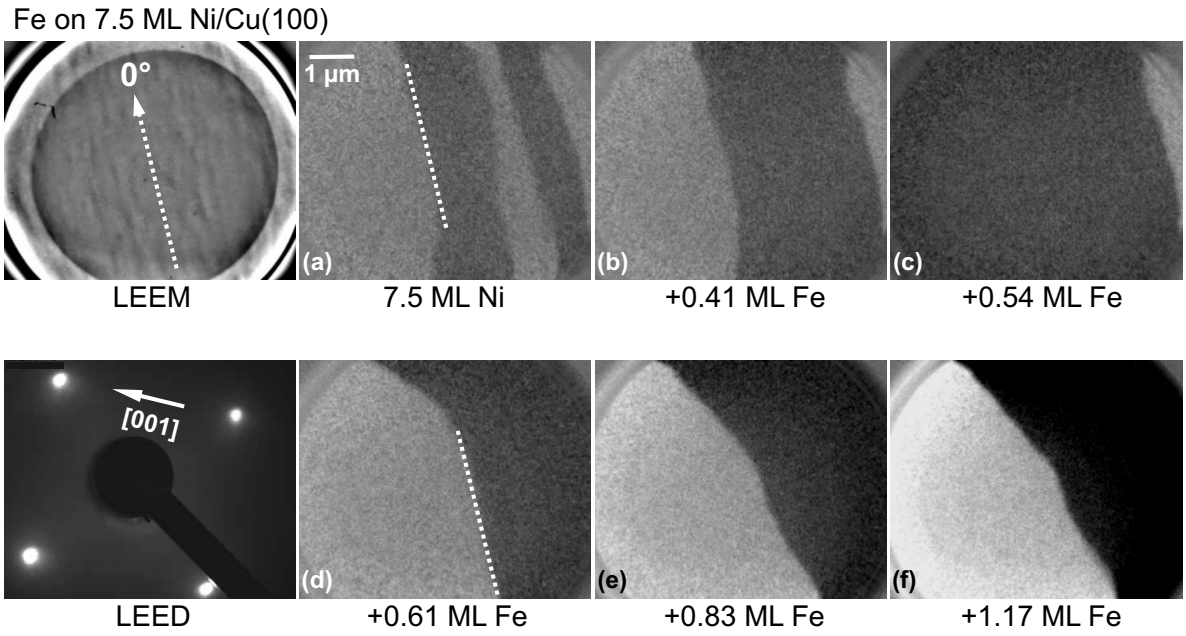

Figure 5.10: Perpendicularly magnetized stripe domains of a 7.5 ML Ni/Cu(100) film have a width of 0.5-3 μm and are pinned along the Cu atomic step edges, as indicated by the white dotted line (a). Addition of 0.5 ML Fe causes a formation of larger domains (b)-(c). At an Fe amount of more than 0.6 ML the domain wall pinning is lifted, and an orientation of the wall without correlation to the topography but along [011] takes place, (d)-(f). Note, that the sample has been moved to a different position in (d).

anisotropy of the Ni underlayer must be responsible for the strong domain wall pinning. The thinner Ni film has a lower effective anisotropy, since the film thickness is still close to the spin-reorientation thickness, where the value of K_2^{eff} becomes small. The larger width of the domain walls found for Fe layers grown on 7.5 ML Ni/Cu(100) compared to bilayers based on 11 ML Ni/Cu(100) is also attributed to the lower anisotropy. Obviously, the pinning of the narrower domain walls is stronger than that of the wider ones. Note, that the wall rotation in the 7.5 ML Ni film is accompanied by the occurrence of slight in-plane contrast, which indicates that the magnetization is tilted against the surface normal. Such spin canting below 1 ML Fe is observed in all studied Fe/Ni bilayers on Cu(100). Due to the increased shape anisotropy and the change of the surface anisotropy, as Fe atoms are adsorbed at the surface, the perpendicular anisotropy of the Ni layer is reduced leading to a canted orientation of the magnetization of the bilayer system.

The identification of the type of domain walls in perpendicularly magnetized Ni/Cu(100) and Fe/Ni/Cu(100) ultrathin films with low Fe coverage turned out to be difficult. Although the magnetization reorientation mechanism is different in Bloch and Néel walls −as discussed in section 1.3− the magnetization in the core of both walls lies parallel to the surface and should give rise to magnetic contrast of the walls in one direction of the electron beam polarization $\mathbf{P}$ within the film plane. However, no magnetic contrast of the domain walls within the film plane

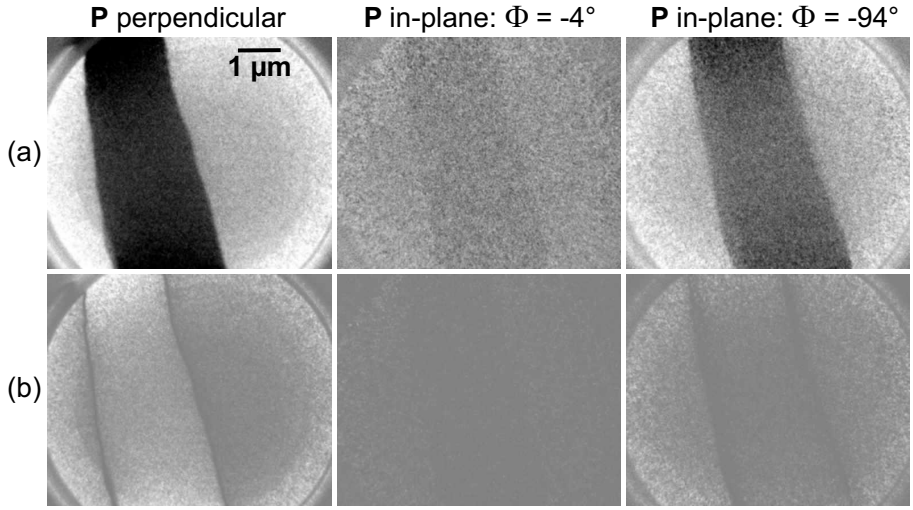

Figure 5.11: (a) Original SPLEEM images of an $Fe_{0.7}/Ni_{11}/Cu(100)$ at three different orientations of the beam polarization $\mathbf{P}$ and (b) the corresponding modified images, in which areas are accented which do *not* show any magnetic contrast in the SPLEEM images above. Only in the images with $\mathbf{P}$ perpendicular to the surface and $\mathbf{P}$ along $\Phi = -94°$ in-plane the domain walls are visible in (b), indicating that the magnetic moments do *not* point into these directions but along the domain wall. The walls are Bloch walls.

of Ni/Cu(100) and Fe/Ni/Cu(100) films with an Fe layer thickness below 1.75 ML is observed. Weak MC of the walls occurs for the first time at 1.75 ML Fe in the SPLEEM images taken at $\Phi = -4°$, and no MC in the walls is detected at $\Phi = -94°$. In the Fe thickness range of 1.75 ML to 2.5 ML magnetic contrast occurs in the domain walls of the images detecting the in-plane component of the magnetization along the domain walls ($\Phi = -4°$ orientation), but no in-plane MC within the walls is found perpendicular to this direction ($\Phi = -94°$ orientation of $\mathbf{P}$). In Fig. 5.11 (a) original SPLEEM images of an $Fe_{0.7}/Ni_{11}/Cu(100)$ film at three different orientations of $\mathbf{P}$ and the corresponding modified images (b), in which areas are accented which do *not* show any magnetic contrast in the SPLEEM images above (i. e. the domain walls and the background outside the circular field of view) are presented. Only in the modified images (b) with $\mathbf{P}$ perpendicular to the surface and $\mathbf{P}$ oriented in-plane along $\Phi = -94°$ the domain walls are visible, which indicates that the magnetization does *not* point into these directions. No dark lines are seen in the image with $\mathbf{P}$ oriented in-plane along $\Phi = -4°$ (b), which indicates that the magnetization in the wall must be aligned parallel to the wall. Since in this Fe thickness range the film is out-of-plane magnetized with a polar angle of $\theta \approx 15°$, these domain walls are identified as Bloch walls. In Fig. 5.12 the in-plane component of the canted magnetization pointing along the Bloch wall is imaged. Interestingly, the chirality of both walls changes as the Fe thickness is increased from 1.75 ML to 2.5 ML, where the domain splitting indicates the beginning of the spin-reorientation transition. As will be discussed in chapter 6 the Bloch walls turn into Néel walls during the SRT.

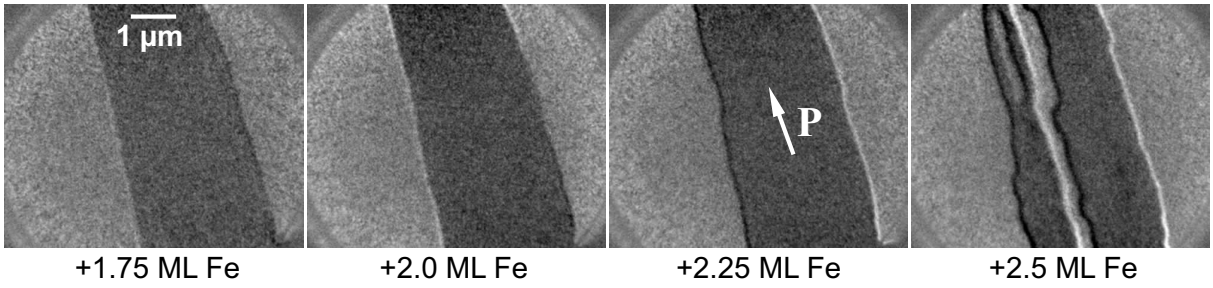

Figure 5.12: Evolution of Bloch walls of an $Fe_x/Ni_{11}/Cu(100)$ film as a function of the Fe layer thickness x. Imaged is the magnetization component pointing into $\Phi = -4^\circ$ within the film plane as indicated by the white arrow and $\mathbf{P}$. At 1.75 ML Fe magnetic contrast occurs in the domain wall and increases up to 2.5 ML Fe. Interestingly, the chirality of both walls changes from 1.75 to 2.25 ML Fe coverage. No magnetization component of the wall within the film plane is observed at $\Phi = -94^\circ$ (perpendicular to the wall) below 2.5 ML Fe, indicating the sense of magnetization reorientation of a Bloch wall.

It remains unclear why there is no in-plane MC of the domain walls of the 11 ML Ni/Cu(100) film. One might argue that the perpendicular anisotropy of the film is so large that according to $w = 2\sqrt{A/K_{\text{eff}}}$ the wall width w becomes too small to be resolved. Using the anisotropy constants $K^V_{2,Ni}$ and $K^S_{2,Ni-Cu}$ from table 6.3 and $K^S_{2,Ni-vac} = -159$ μeV/atom from [83] and 7.5 μeV/atom [9] for the shape anisotropy yields a domain wall width of ≈30 nm. This result could indeed mean that the wall is too narrow to be resolved, since it is close to the best resolution of 10 nm of the SPLEEM. However, the measurement of the wall width of the domains in the images with $\mathbf{P}$ normal to the surface yields ≈130 nm, which is in clear contradiction to the calculated width. The idea to extrapolate the wall width, derived from the images with $\mathbf{P}$ oriented in-plane along $\Phi = -4^\circ$ and $\Phi = -94^\circ$, from 2.5 ML Fe down to 0 ML Fe, in order to determine the wall width of the 11 ML Ni/Cu(100) film also did not confirm a wall width around 30 nm. Furthermore, the wall width in the images with $\mathbf{P}$ oriented in-plane do not show a monotonic dependence as a function of the Fe thickness, but they remain rather constant at 130 nm within an error of ± 10 nm. This confirms the width measured in the domain image probing the normal magnetization component of 11 ML Ni/Cu(100). A vanishing domain wall MC in the film plane may be due to the small magnetic moment of Ni. It shall be noted, that even the expected in-plane magnetic contrast of films in the thickness range of 5 to 7 ML was not detected on the used Cu(100). A theoretical explanation that the wall is a vortex wall with a Néel cap, in which the in-plane projection of magnetic moments pairwise compensated each other and thus yield a net magnetic moment near zero within the wall, is rather improbable, since such vortex walls are more likely to appear in thicker films, e. g. 100 nm Permalloy [17].

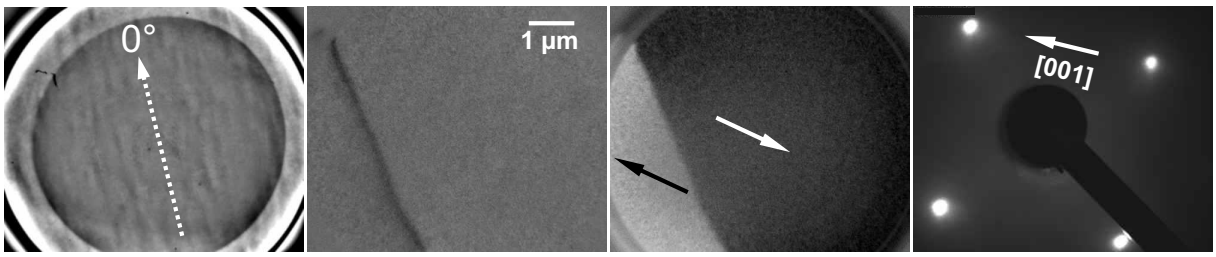

Figure 5.13: In-plane magnetized $Fe_{2.8}/Ni_{7.5}$ /Cu(100) film at 300 K. At $\Phi = -141°$ the magnetic contrast vanishes and the Néel wall is revealed by dark contrast. The arrows indicate the direction of the magnetization, which is collinear to the [001] crystallographic axis, as confirmed by the LEED image taken at an energy of the electrons of 150 eV.

5.3.2 In-plane magnetized domains (> 2.8 ML Fe)

Fe/Ni bilayers on Cu(100) with Fe cap layers above 3 ML are magnetized in the film plane for all Ni layer thicknesses studied (1.5 ML to 11 ML). The domain size is found to be on the order of 10 μm. The magnetization direction with respect to the crystallographic axes was checked by low energy electron diffraction. In agreement with the expectation for the easy axis of the magnetization of Fe films grown on Cu(100), which is [001], the easy axis of the $Fe_{2.8}/Ni_{7.5}$/Cu(100) film is collinear to the [001] crystal axis. It should be noted that the LEED system was installed after the measurement, and only for this measurement the crystallographic orientation of the Cu(100) substrate was determined. Fig. 5.13 illustrates the determination of the magnetization direction in the film plane. With the electron beam polarization directed in the plane ($\theta = 90°$) the azimuthal angle Φ was varied until the magnetic contrast in both domains vanished at $\Phi = -141°$. Since $MC \propto \mathbf{P} \cdot \mathbf{M}$ the easy direction is collinear to the orientation $\Phi = -51°$. The magnetization vectors within the two domains are anti-aligned as indicated by the arrows, and they are parallel to the [001] direction, which is confirmed by the LEED pattern taken at an energy of the electrons of 150 eV. The domain wall, however, seems to be pinned although it does not exactly run parallel to the Cu atomic steps as shown in Fig. 5.10. The width of the domain wall is 215 ± 10 nm, which is the same as measured for the perpendicularly magnetized underlayer with and without Fe cap layers up to 2.25 ML. From the dark MC of the domain wall at $\Phi = -141°$ in Fig. 5.13 it is clear, that the magnetization within the wall rotates in the film plane, which is characteristic for a Néel wall.